

## **A new inductance estimator based on Lagrange Form polynomials for real-time switched reluctance machine control**

**Um novo estimador de indutância baseados em polinômios de Lagrange para controle em tempo real da máquina a relutância variável**

**Un nuevo estimador de inductancia basado en polinomios en forma de Lagrange para el control de máquinas de relutancia conmutada en tiempo real**

Received: 03/22/2022 | Reviewed: 03/29/2022 | Accept: 03/31/2022 | Published: 04/08/2022

**Ricardo Tirone Fidelis**

ORCID: <https://orcid.org/0000-0002-0693-3659>  
Federal University of Uberlandia, Brazil  
E-mail: [ricardotirone@gmail.com](mailto:ricardotirone@gmail.com)

**Victor Henrique da Cunha Faria**

ORCID: <https://orcid.org/0000-0003-0063-6319>  
Federal University of Uberlandia, Brazil  
E-mail: [victorhcf@ufu.br](mailto:victorhcf@ufu.br)

**Marcos José de Moraes Filho**

ORCID: <https://orcid.org/0000-0001-5545-3566>  
Federal University of Uberlandia, Brazil  
E-mail: [marcos.jmf@hotmail.com](mailto:marcos.jmf@hotmail.com)

**Ghunter Paulo Viajante**

ORCID: <https://orcid.org/0000-0001-6006-491X>  
Federal University of Uberlandia, Brazil  
E-mail: [ghunterp@gmail.com](mailto:ghunterp@gmail.com)

**Eric Nery Chaves**

ORCID: <https://orcid.org/0000-0003-0233-2570>  
Federal Institute of Goiás, Brazil  
E-mail: [Eric.neryx@gmail.com](mailto:Eric.neryx@gmail.com)

**Augusto Wohlgemuth Fleury Veloso da Silveira**

ORCID: <https://orcid.org/0000-0003-3628-3930>  
Federal University of Uberlandia, Brazil  
E-mail: [augustofleury@ufu.br](mailto:augustofleury@ufu.br)

**Luciano Coutinho Gomes**

ORCID: <https://orcid.org/0000-0002-2827-6944>  
Federal University of Uberlandia, Brazil  
E-mail: [lcgomes@ufu.br](mailto:lcgomes@ufu.br)

### **Abstract**

This paper presents a new methodology for modeling the inductance curves of switched-reluctance machines using cubic splines based on Lagrange form polynomials. The proposed methodology allows for the estimation of the instantaneous inductance and derivative of the inductance in each phase of the machine. All steps of the proposed methodology are presented and discussed, detailing the information necessary for its use. The results of an experimental and computational simulation, both as a motor and a generator, are presented and discussed, and the estimated curves are compared with the design curves of each result. The inductance estimator was embedded in a low-cost DSP, and the machine was driven using an experimental bench. The experimental results are presented and compared with the simulation results, allowing for the evaluation of the accuracy level obtained by the proposed estimator. The estimator combines precision with low computational cost, which makes this method a strong candidate for systems that require estimation of machine parameters in real time, such as torque and flux, permitting the implementation of new control techniques.

**Keywords:** Switched reluctance machine; Inductance estimator; Cubic splines; Lagrange form polynomials.

### **Resumo**

Este artigo apresenta uma nova metodologia para modelagem de curvas de indutância de máquinas de relutância chaveada usando splines cúbicos baseados em polinômios da forma de Lagrange. A metodologia proposta permite estimar a indutância instantânea e derivada da indutância em cada fase da máquina. Todas as etapas da metodologia proposta são apresentadas e discutidas, detalhando as informações necessárias para sua utilização. Os resultados de uma simulação experimental e computacional, tanto como motor quanto como gerador, são apresentados e discutidos, e as

curvas estimadas são comparadas com as curvas de projeto de cada resultado. O estimador de indutância foi embarcado em um DSP de baixo custo, e a máquina foi acionada usando uma bancada experimental. Os resultados experimentais são apresentados e comparados com os resultados da simulação, permitindo avaliar o nível de precisão obtido pelo estimador proposto. O estimador combina precisão com baixo custo computacional, o que torna este método um forte candidato para sistemas que requerem estimativa de parâmetros da máquina em tempo real, como torque e fluxo, permitindo a implementação de novas técnicas de controle.

**Palavras-chave:** Máquina de relutância comutada; Estimador de indutância; Splines cúbicos; Polinômios de Lagrange.

### Resumen

Este artículo presenta una nueva metodología para modelar las curvas de inductancia de máquinas de relutancia conmutada utilizando splines cúbicos basados en polinomios de forma de Lagrange. La metodología propuesta permite estimar la inductancia instantánea y la derivada de la inductancia en cada fase de la máquina. Se presentan y discuten todos los pasos de la metodología propuesta, detallando la información necesaria para su uso. Se presentan y discuten los resultados de una simulación experimental y computacional, tanto de motor como de generador, y se comparan las curvas estimadas con las curvas de diseño de cada resultado. El estimador de inductancia se incrustó en un DSP de bajo costo y la máquina se condujo utilizando un banco experimental. Los resultados experimentales se presentan y comparan con los resultados de la simulación, lo que permite evaluar el nivel de precisión obtenido por el estimador propuesto. El estimador combina precisión con bajo costo computacional, lo que hace de este método un fuerte candidato para sistemas que requieren estimación de parámetros de máquina en tiempo real, como torque y flujo, permitiendo la implementación de nuevas técnicas de control.

**Palabras clave:** Máquina de relutancia conmutada; Estimador de inductancia; Splines cúbicos; Polinomios en forma de Lagrange.

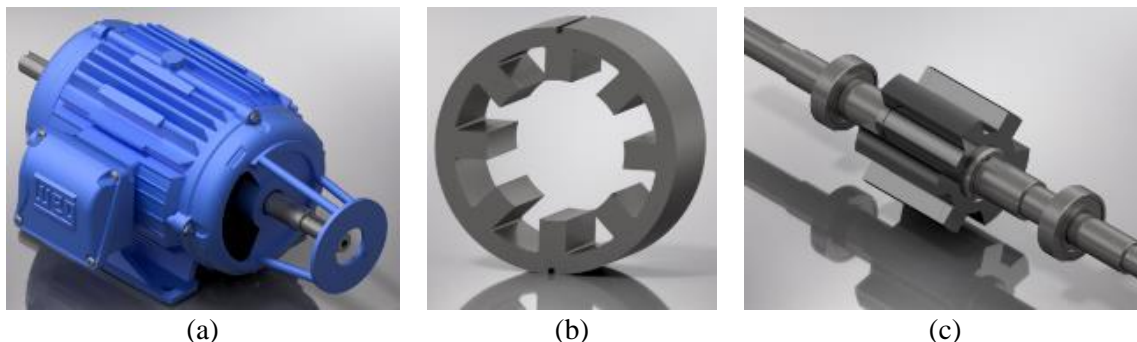
## 1. Introduction

Over recent decades, electric machine drive systems have seen rapid development, showing significant advances in terms of efficiency, precision, and converted power. Through such development, new machines have become a part of alternatives that are applicable to drive systems at variable speeds. In this context, switched reluctance machines (SRMs) have become attractive.

Compared to other types of machines, the SRM exhibits superior performance when operating under high-speed and high-temperature conditions. This advantage is mainly due to the lack of rotor windings or permanent magnets. In addition, it has a low temperature influence, as the rotor is made only of laminated steel, and it also possesses magnetic permeability, which is not heavily influenced by temperature (Bilgin et al., 2019).

From a constructive point of view, the SRM stands out for having salient poles in both the rotor and stator, and the absence of permanent windings or magnets in the rotor, a characteristic that contributes to the reduction of ohmic losses, which allows for a simple construction. It is a robust and reliable machine that tolerates phase faults in polyphasic machines and the possibility of working under adverse conditions and environments, as well as retaining a good torque/volume ratio and low-cost construction. Figure 1 displays an  $8 \times 6$  SRM structure. Figure 1(a) shows the general SRM structure, Figure 1(b) shows the stator, and Figure 1(c) depicts the rotor.

**Figure 1.** View of  $8 \times 6$  SRM.



Source: Moraes Filho (2017).

Owing to the electrical, magnetic, and mechanical characteristics of the machine, and the interactions between the magnetic circuits of the rotor and stator, the inductance exhibits nonlinear behavior and is strongly dependent on the rotor position and the current applied in each phase (Viajante et al., 2016, & Corda et al., 1980, & Takayoshi et al, 1997, & Mikail et al, 2013). Figure 2 shows the inductance surface as a function of the phase current and mechanical rotor position for the studied machine, obtained using the finite element method (FEM), from the SRM project. This figure highlights that the phase inductance depends on the operating conditions of the machine. This characteristic leads to a challenging situation associated with machine control, regarding its use in applications such as motors and generators (Bilgin et al, 2019, & Emadi et al., 2008).

However, the challenges associated with the complexity of this machine are also the motivators of several scientific studies, which always look toward solutions that mitigate such problems, many of which are related to the concept of a precise machine dynamic model (Kushwaha et al, 2020, & kalaivani at al, 2013, & Nguyen et al, 2019, & Yasa et al, 2018). In this respect, several studies have been proposed with the objective of obtaining robust and reliable models; however, the vast majority of these are dependent on the lookup table that contains the inductance surface, requiring that the model seeks the inductance value through two-dimensional interpolation at each instant of processing. Such models become prohibitive in embedded systems, as they require a high computational effort, making it difficult or even impossible to embed them in low-cost digital systems such as digital signal processors (DSPs) or field programmable gate arrays (FPGAs).

Andrade and Krishnan (2001) presented an analytical model for SRM inductance curves through the expansion of the Fourier series. This modeling is strongly dependent on the pre-established profile for inductance, in addition to requiring relevant computational effort, making it unfeasible as a tool to control the machine in real time. This method has satisfactory precision in simulations, which represents an advance in the replacement of lookup tables by analytical methods.

Velmurugan & Yeoh (2019) presented a model for the SRM inductance dividing the curve into segments and modeling each segment according to its linearity, attributing to the linear regions a modeling through the equation of a straight line, in which third-order Fourier series are applied, resulting in a set of coefficients for each curve segment. The modelling approach, using the inductance profile presented in (Velmurugan, 2019), provides a highly accurate model that can be used for computational simulation studies, the use of this technique in real-time drive systems can be problematic, as it requires the calculation and solution of the Fourier series, which are calculations that require considerable computational effort.

A nonlinear flux linkage model on a 2-D plane was proposed (Cai at al, 2010) using a neural network with a set obtained experimentally from a planar switched reluctance machine (PSRM) system. The proposed nonlinear modeling of the flux linkage on a 2-D plane is appropriate for precision positioning applications of PSRM.

Banerje and Sensarma proposed a mathematical model for the nonlinear flux linkage characteristics of an SRM (Benerjee, 2018). In the proposed model, three coefficients are determined using an approximate analytical method and regression analysis. This model is useful for the estimation of angles to activate the phases of the SRM with an estimation error of less than four mechanical degrees.

An efficient modeling technique for a fully pitched linear switched reluctance machine (LSRM) and drives was presented in (Du at al., 2010). Next, a finite element analysis was performed to verify the feasibility of the mathematical method. The FEA results are in good agreement with the numerical simulation results.

In (Rajib at al., 2013), a method of modeling the SRM including mutual coupling effects is presented, which incorporates the mutual coupling effect, obtaining results such as FEA, which is useful for analysis, projects, and simulation of SRM.

Cai & Liu (2020) presented an inductance estimation that mitigates the effects of magnetic saturation by using the injection of high-frequency signals in the SRM phases, although this does not accurately estimate inductance, it is indicated for SRM sensorless drives.

A universal sensorless starting scheme that considers the magnetic saturation effect is proposed for controlling SRM drives (Lin et al., 2014). The full-cycle unsaturated inductance can be reconstructed from the saturated incremental inductance in real time via inductance data acquisition. The proposed work presents a good level of precision in the estimation of unsaturated inductance and is applicable to sensorless drive techniques.

A study is presented on an inductance estimator for the LSRM (Wang et al. 2016), which considers the losses in iron using the injection of current pulses in the machine phases. The authors present good results, but the inductance obtained does not consider the saturation effects as being useful for sensorless applications.

In (Sahoo et al., 2008), an analytical model was proposed for the SRM phase flux linkage, which was divided into four regions according to the physical characteristics. A two-stage polynomial fitting approach was used to capture each region. Each region was captured using 36 parameters and 144 coefficients. Through these constraints, it is possible to estimate the instantaneous torque with an average computational weight.

Matrix operations and parabolic regression were used to obtain an accurate estimator. This method demands the supply of voltage in the four phases of the SRM simultaneously, which makes it difficult to apply it in real-time SRM driving because all phases must be switched off during data measurement.

The scientific community seeks ways to estimate or calculate inductance along with other parameters by applying different techniques and strategies aimed at driving and control applications. This makes it essential to obtain a robust and precise mathematical model, which also allows inductance and other parameters to be used in computational and experimental applications. With the method developed and presented in this article, it is possible to implement new controls or improve controls currently used, such as those presented in (Fang, 2020) in which the SRM switching angles for electric vehicles are optimized, in (Pomming, 2020) a way to calculate the magnetic field for SRM is presented and (Song, 2019) a way to get direct instantaneous Torque based on modular level power converter.

In the following sections, a new method of inductance estimation is presented. The methodology presented obtains the inductance through the resolution of some third-order polynomials, which are modeled using cubic splines obtained from the Lagrange model. All the steps for obtaining the polynomial are presented in detail, thus allowing for the reproduction of the method for other machines. The simulation results for the machine operating as the generator and motor are also presented and compared with the design curves from the SRM, and the experimental results obtained in a drive for an  $8 \times 6$  SRM acting as a generator are presented and compared with the simulation results.

## 2. Induction Functions Modeling Methodology

The methodology developed in this work consists of establishing an inductance calculation function,  $L(i, \theta)$ , which considers two input parameters: current in phase,  $i$ , and rotor angular position,  $\theta$ . The proposed method consists of surveying analytical functions using Lagrange polynomials that represent the inductance variation as a function of the current and the variation of the inductance as a function of the angular position.

The methodology is described in six steps. All the steps that constitute the methodology developed in this study are described and analyzed below.

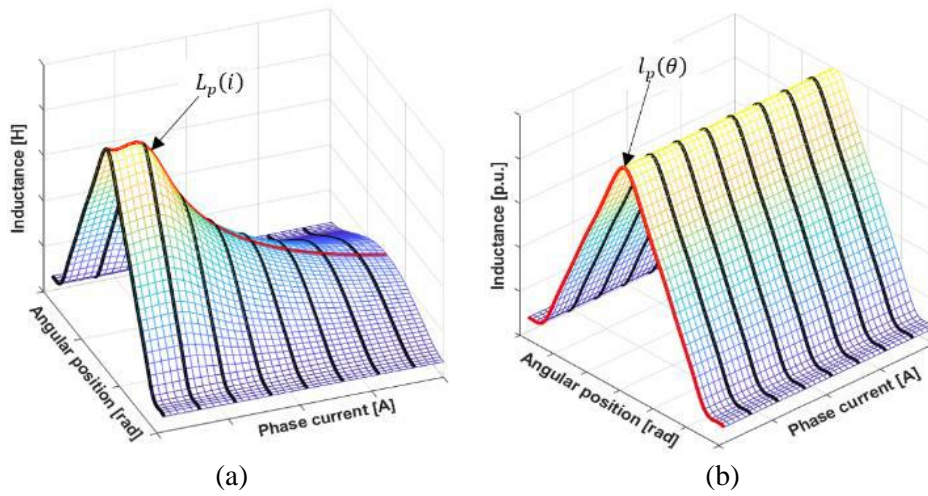
**Step I:** Calculation and analysis of surface  $L(i, \theta)$ . It is necessary to ensure that this surface is correctly calculated, as all the following steps depend on it, and the curves used as a reference for this work were obtained through the finite element method.

**Step II:** inductance curve determination for the rotor position completely aligned to the stator,  $L_p(i)$ , which is the maximum inductance curve for all current points. This curve is highlighted in figure 02-a a.

**Step III:** Determination of inductance curve as a function of rotor position: The process is initially performed by applying Equation 01, where the inductance surface is divided into curves  $L(i_k, \theta)$  for each current being studied. Each curve was divided according to the corresponding value of  $L_p(i)$ , point to point. As a result, surface  $l(i, \theta)$  is obtained, which has dimensionless values that are smaller than the unit.

$$l(i_k, \theta) = \frac{L(i_k, \theta)}{L_p(i_k)}, \text{ para } i_1, i_2, \dots, i_k, \dots, i_{max} \quad (1)$$

**Figure 2.** Inductance surfaces as a function of the current and the mechanical position of the rotor. (a) Highlighting curve  $L_p(i)$ ; (b) highlighting curve  $L_p(\theta)$ .



Source: Authors.

Figure 2(a) shows the inductance surface obtained by the finite element method with the curve for the maximum inductance as a current function, and Figure 2(b) shows the surface  $l(i, \theta)$ . It is noteworthy that with the proposed methodology, surface  $l(i, \theta)$  presents values for the resulting curves with a similar profile for all current positions. Therefore, this methodology allows only one profile to be used as a reference for the inductance variation in relation to the angular position  $l_p(\theta)$ .

Therefore, after the execution of step III, the  $L(i, \theta)$  surface is modeled from the composition of the two curves  $L_p(i)$  and  $l_p(\theta)$ , according to the equation in the matrix form, as presented in (2).

$$L(i, \theta) = [L_p(i)]^T \times [l_p(\theta)] \quad (2)$$

**Step IV:** Mathematical modeling, performed through cubic splines based on Lagrange polynomials, is applied to the encountered curves,  $L_p(i)$  and  $l_p(\theta)$ . The choice of this method is justified, as it is immune to the effects of the Runge phenomenon, does not require an equal distance between the points, does not present the drawbacks of the Stone-Weirstrass approximation theorem, and still presents curves for which the derivatives are continuous at all operating points.

Accordingly, a polynomial is defined for each interval  $[x_{k-1}, x_k]$ , where the final function is a third-order polynomial at each interval, as shown in (3). The total number of polynomials depends on the complexity of the curve to be modeled and the desired level of precision.

$$\ell(x) = \begin{cases} \ell_1(x), x_0 \leq x \leq x_1 \\ \ell_2(x), x_1 \leq x \leq x_2 \\ \vdots \\ \ell_k(x), x_{k-1} \leq x \leq x_k \\ \vdots \\ \ell_n(x), x_{n-2} \leq x \leq x_{n-1} \\ \ell_n(x), x_{n-1} \leq x \leq x_n \end{cases} \quad (3)$$

For each of the polynomials  $\ell(x)$  it is necessary to determine four coefficients  $a_2, a_1$  and  $a_0$ , as  $a_3 \neq 0$ . According to (6), (7), and (8),  $\ell(x)$  is the inductance as an input parameter function,  $x$ .

$$\frac{d^2 \ell}{dx^2} = \ell''(x) = 6 \cdot a_3 \cdot x + 2 \cdot a_2 \quad (4)$$

$$\frac{d \ell(x)}{dx} = \ell'(x) = 3 \cdot a_3 \cdot x^2 + 2 \cdot a_2 \cdot x + a_1 \quad (5)$$

$$\ell(x) = a_3 \cdot x^3 + a_2 \cdot x^2 + a_1 \cdot x + a_0 \quad (6)$$

Cubic spline modeling using the Lagrange method begins with the second derivative of the polynomial, which is a linear function. The linear curve was modeled using the Lagrange method, as shown in Eqs. (7).

$$\ell''(x) = \sum_{k=1}^n \text{Lagrange}_k(x) \cdot y_k \quad (7)$$

$$\text{Lagrange}_k(x) = \prod_{j=1, j \neq i}^n \frac{(x-x_j)}{(x_k-x_j)} \quad (8)$$

$$\ell''(x) = \frac{x-x_{k+1}}{x_k-x_{k+1}} \ell''(x_k) + \frac{x-x_k}{x_{k+1}-x_k} \ell''(x_{k+1}) \quad (9)$$

The third-order polynomial in the  $k$  interval can be determined by integrating the equation twice. The resulting expression contains two integration constants. These two constants can be determined from the boundary conditions presented in (10), (11), and (12).

The second derivative values at the start and end points of the interval for the  $(n - 2)$  inner points can be deduced from the first-derivative continuity of the adjacent interval polynomials at the inner points.

$$\ell'_k(x_{k+1}) = \ell'_{k+1}(x_k) ; \text{for } k = 1, 2, \dots, n - 2 \quad (10)$$

The function value is known at the end of each segment, as shown in (11) and (12).

$$\ell(x) = y_k \quad (11)$$

$$\ell(x_{k+1}) = y_{k+1} \quad (12)$$

Once the integration constants are determined, one can proceed to the development stage through the processes of integration and algebraic manipulation, as shown in (15) for  $x_k \leq x \leq x_{k+1}$  and  $k = 1, 2, 3, \dots, n - 1$ , by considering  $h_k$  as the spacing of the points on the  $x$ -axis, as shown in (13) and (14), which do not need to be equally spaced for the Lagrange method.

$$h_k = x_{k+1} - x_k \quad (13)$$

$$\delta_k = \ell''(x_k) \quad (14)$$

Writing the expressions in terms of  $\ell_k(x)$  and  $\ell_{k+1}(x)$ , calculating the derivatives of these expressions and replacing these derivatives in (10) results in (16).

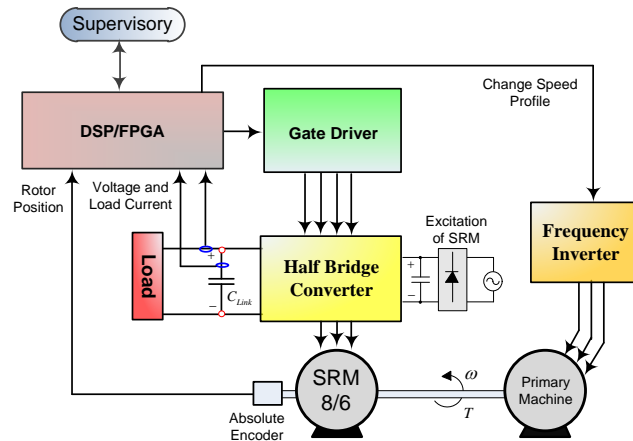
From (16), a system with  $n-2$  equations needs to be solved for the terms  $\ell_k''(x_k)$ . The system is expressed as (17).

$$\ell_i(x) = \frac{\delta_k}{6h_k} (x_{k+1} - x)^3 + \frac{\delta_{k+1}}{6h_k} (x - x_k)^3 + \left[ \frac{y_k}{h_k} - \frac{\delta_k h_k}{6} \right] \cdot (x_{k+1} - x) + \left[ \frac{y_{k+1}}{h_k} - \frac{\delta_{k+1} h_k}{6} \right] \cdot (x - x_k) \quad (15)$$

$$h_k \delta_k + 2(h_k + h_{k+1}) \delta_{k+1} + h_{k+1} \delta_{k+2} = 6 \left( \frac{y_{k+2} - y_{k+1}}{h_{k+1}} - \frac{y_{k+1} - y_k}{h_k} \right) \quad (16)$$

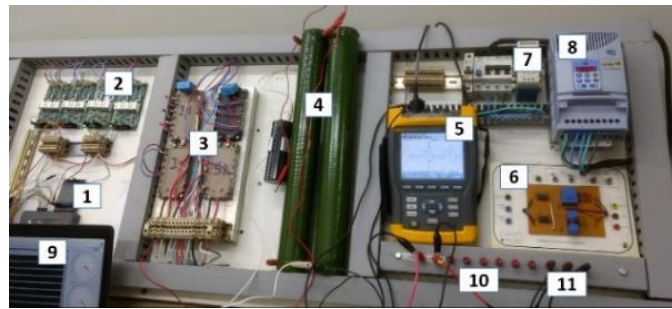


**Figure 3.** Experimental Setup and Simulation Block Diagram.



Source: Viajante (2018)

**Figure 4.** Experimental workbench.



Source: Authors.

**Table 1.** Experimental setup components.

ID	DESCRIPTION
1	NY MyRIO 1900
2	Isolated drive supplier
3	Half bridge converter
4	Capacitor and resistor
5	Power analysis instrument
6	Voltage/current conditioner
7	Source for peripherals
8	Frequency inverter
9	Computer / Supervisory
10	SRM out pins
11	MIT out pins

Source: Authors.

### a) Determining of polynomials

To determine the inductance function coefficients,  $\ell_p(i)$ ,  $\ell_\theta(\theta)$  and  $\mathcal{L}(i, \theta)$ , nine points were used for the angular position and five points for the current, chosen arbitrarily, in order to better accommodate the original curve variations, which aim to optimize model accuracy and reduce computational effort, as shown in Figures 5(a) and 5(b). For the present case study,  $\ell_\theta(\theta)$  polynomials are used because of the mirroring effect of the curve in the rotor/stator alignment position and four

polynomials for  $\ell_p(i)$ . The data that must be loaded into the SRM DSP drive system are shown in the following tables: Table 2 coefficient for the  $\ell_\theta(\theta)$  polynomials and Table 3 coefficient for the  $\ell_p(i)$  polynomials.

Obtaining the inductance derivative is also possible using the same coefficients because the Lagrange polynomials have a continuous derivative throughout the modeling domain. As it is a partial derivative of the angular position, the functions modeled for the current can be considered constant, resulting in (26).

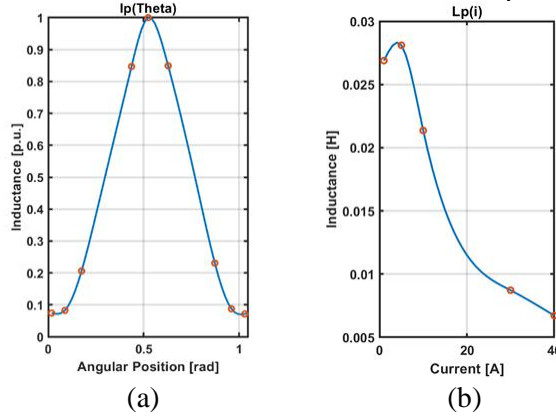
$$\mathcal{L}(i, \theta) = \ell_p(i) \cdot \ell_\theta(\theta) \quad (23)$$

$$\frac{\partial \mathcal{L}(i, \theta)}{\partial \theta} = \ell_p(i) \frac{\partial(\ell_\theta(\theta))}{\partial \theta} \quad (24)$$

$$\frac{\partial(\ell_\theta(\theta))}{\partial \theta} = 3 \cdot a_1 \cdot \theta^2 + 2 \cdot a_2 \cdot \theta + a_3 \quad (25)$$

$$\frac{\partial \mathcal{L}(i, \theta)}{\partial \theta} = \ell_p(i) (3 \cdot a_1 \cdot \theta^2 + 2 \cdot a_2 \cdot \theta + a_3) \quad (26)$$

**Figure 5.** Points used to determine polynomials. (a) determination of  $\ell_p(i)$ ; (b) determination of  $\ell_\theta(\theta)$ .



Source: Authors.

**Table 2.** Polynomial coefficient  $\ell_p(\theta)$

Interval	$a_3$	$a_2$	$a_1$	$a_0$
$0 < \theta \leq \frac{\pi}{36}$	52.1812	-2.7322	-0.0896	0.0764
$\frac{\pi}{36} < \theta \leq \frac{2\pi}{36}$	-21.1821	16.4743	-1.7657	0.1252
$\frac{2\pi}{36} < \theta \leq \frac{3\pi}{36}$	0.5026	-0.5569	2.6930	0.2639
$\frac{3\pi}{36} < \theta \leq \frac{4\pi}{36}$	-98.2278	128.6810	-53.6976	7.9378
$\frac{4\pi}{36} < \theta \leq \frac{5\pi}{36}$	Consider the angular position $(\theta - \frac{\pi}{6})$			

Source: Authors.

**TABLE 3.** POLYNOMIAL COEFFICIENT  $\ell_p(i)$

Interval	$b_3$	$b_2$	$b_1$	$b_0$
$1 < i < 5$	-2.463e-5	7.391e-5	6.230e-4	0.0262
$5 < i < 10$	2.462e-5	6.650e-4	0.0043	0.0201
$10 < i < 30$	1.279e-6	1.121e-4	-0.0035	0.0460
$30 < i < 40$	9.988e-8	-1198e-5	2.692e-4	0.0087

Source: Authors

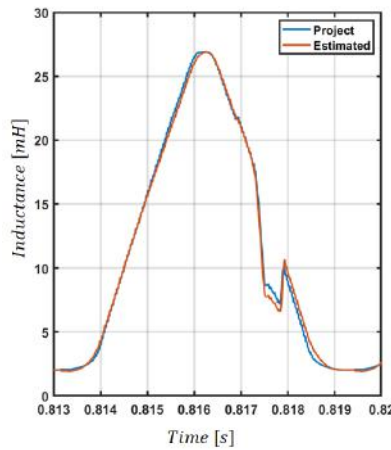
Obtaining these polynomial functions allows the calculation of the inductance value, inductance derivative, torque, flux, and power delivered on the machine axis to be performed in real time with high precision, and can be implemented in embedded systems.

### b) Simulation Results

The simulation of the system was carried out to demonstrate the validity of the proposed methodology for SRM phase inductance estimation in drives operating as motors and generators. Comparing the design inductance and the estimated inductance, the mean square error obtained was less than 5%.

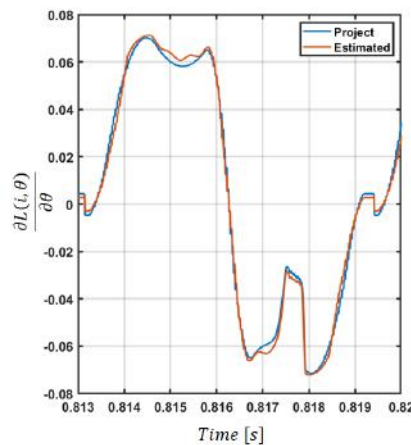
Figure 6 shows a comparison between the inductance curve resulting from the machine design and the inductance curve estimated by the model proposed in the simulation as a generator in an open-loop operation. The curves indicate that the inductance estimator is precise, even under extreme operating conditions. Figure 7 shows a comparison of the curves of the inductance derivatives. This curve is important, as it can be used to estimate several control quantities, including the electromagnetic torque in each machine phase.

**Figure 6.** Comparison between the design curves and estimated by the proposed method for the induction.



Source: Authors.

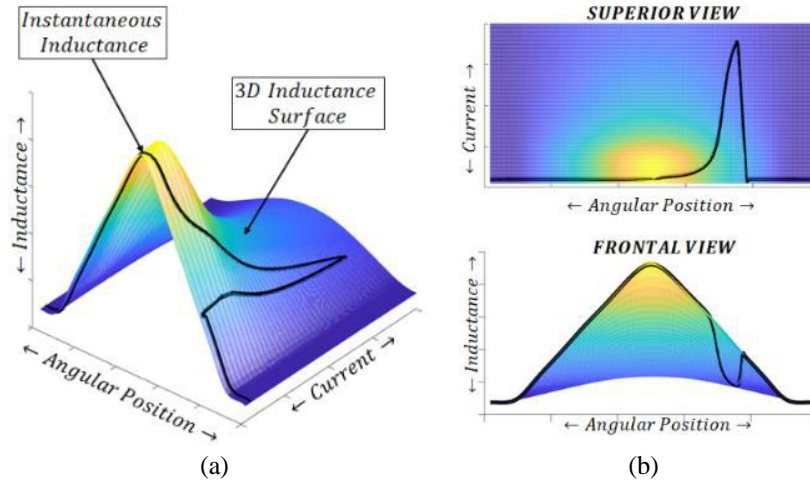
**Figure 7.** Comparison between the design curves and estimated by the proposed method for the derived from induction.



Source: Authors.

Figures 8(a) and 8(b) show the correlation between the design inductance surfaces and the surface estimated by the model proposed in this study. The influence of the current in the instantaneous inductance waveform for the entire operation interval of the machine is presented in Figure 8(a), and all the estimated wave points are on the design surface. Figure 8(b) shows the top and front views of the inductance surface. In these views, one notes that the current peaks cause sags and saturation in the inductance curve. These curves confirm the accuracy of the proposed model, showing that the inductance estimation methodology using cubic spline interpolation based on Lagrange polynomials is adequate for this application.

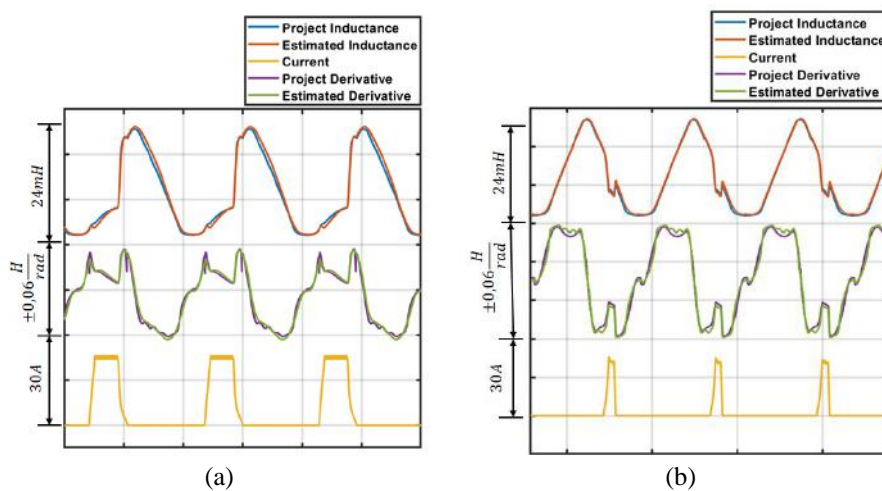
**Figure 8.** Inductance surface and the estimated inductance comparison.



Source: Authors.

Figures 9 (a) and 9 (b) show a comparison between the design inductance and estimated inductance curves, design inductance derivative and estimated inductance derivative, and current for the SRM operating as a motor and for SRM operating as a generator, respectively.

**Figure 9.** Estimated Inductance, derivative and current; (a) Motor Operation; (b) Generator Operation.



Source: Authors.

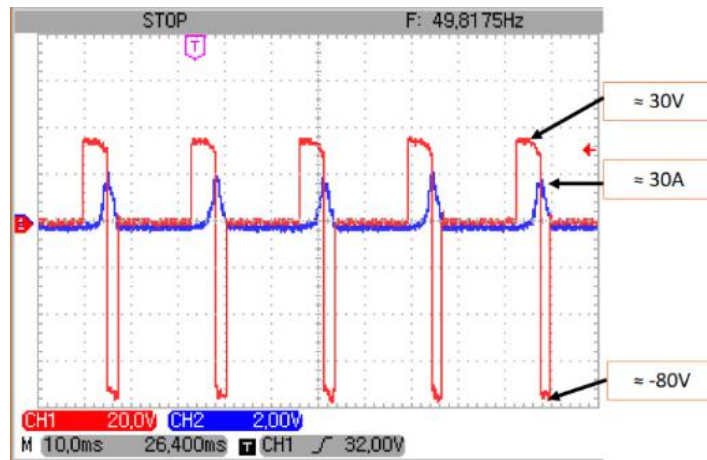
In Figures 9(a) and 9(b), the results show the influence of the phase current on the waveforms of the inductance and its derivative at each SRM operation point. This demonstrates that the proposed model was robust.

### c) Experimental Results

The experimental setup presented in Figures 3 and 4 was used to evaluate the performance and accuracy of the proposed method, which was collected through the DSP analog output and the inductance behavior in real time calculated during activation.

This bench allows for the activation of the SRM as a motor, self-excited generator, and generator with independent excitation. In the results presented, the SRM was driven as a generator operating in an open loop with constant load power, speed, and excitation voltage. Figure 10 shows the voltage and current waveforms measured during the operation as an SRM generator.

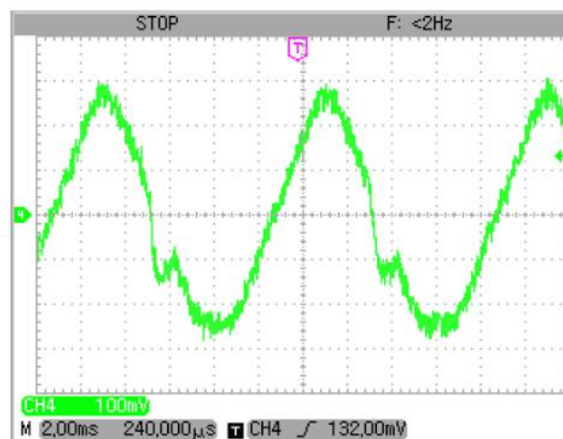
**Figure 10.** SRM phase voltage and current obtained from the experiment.



Source: Authors

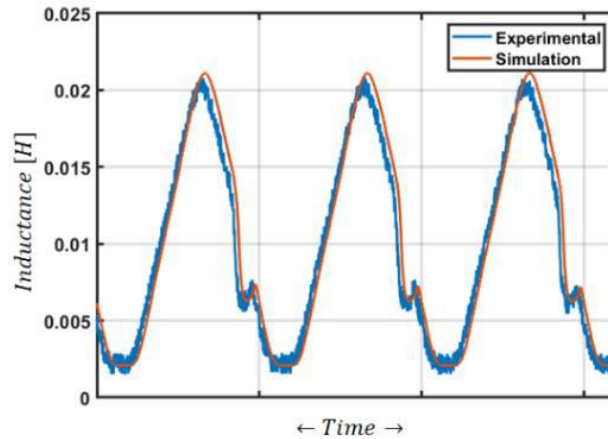
Figure 11 shows the waveforms experimentally obtained for SRM inductance, collected directly at the DSP analog output, and Figure 12 shows the data collected on the oscilloscope printed together with the data obtained from the simulation. It should be noted that the proposed model has a good comparison ratio between the design curve of the machine and the curve drawn directly from the estimator when the real machine is operating.

**Figure 11.** Experimental SRM Inductance obtained from the experiment.



Source: Authors.

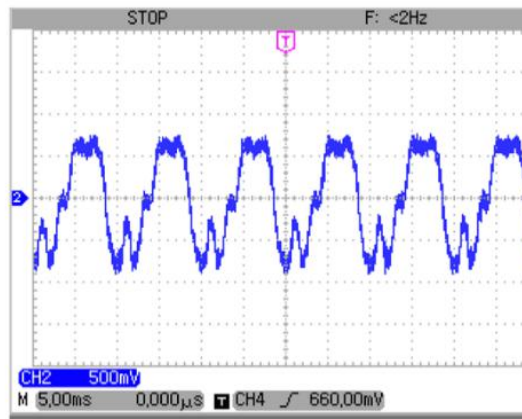
**Figure 12.** Comparison between waveform obtained from simulation and experimental.



Source: Authors.

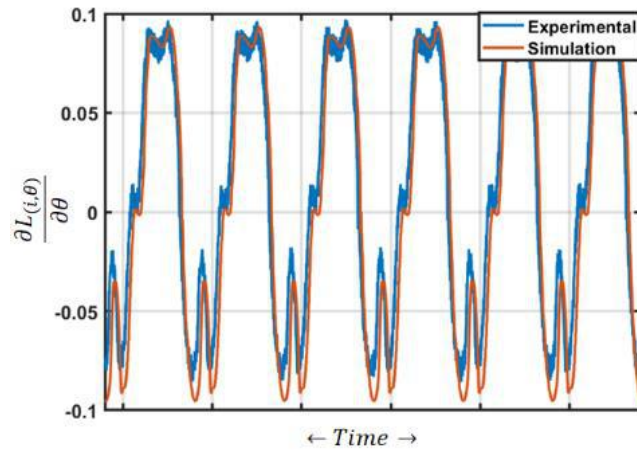
Figure 13 shows the waveforms obtained for the inductance derivative collected directly at the DSP analog output, and Figure 14 shows the data collected on the oscilloscope and compares them with the results obtained in the simulation. It is worth noting that the inductance derivative curve is also precise, which is very important because torque estimation strategies depend directly on this information.

**Figure 13.** Experimental SRM Inductance derivative obtained from the experiment.



Source: Authors.

**Figure 14.** Comparison between waveform obtained from simulation and experimental.



Source: Authors.

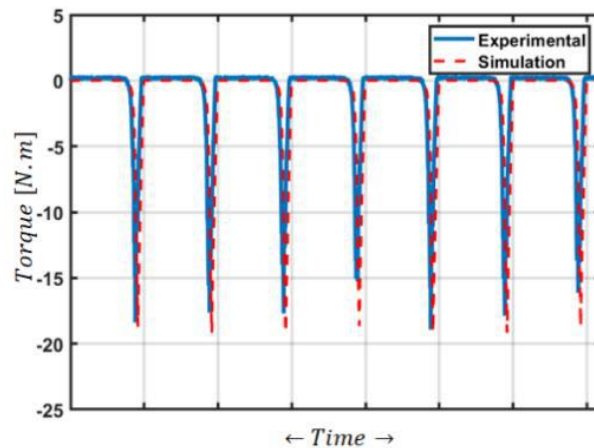
Figure 15 presents the waveform obtained for the estimated electromagnetic torque read directly at the DSP analog output. This torque is based on the inductance derivative calculated using the proposed method. Figure 16 presents a comparison of the estimated torque in real time with the torque extracted from the simulated model. Note that this comparison attests to the good dynamic performance of the proposed model.

**Figure 15.** Experimental SRM torque obtained from the experiment.



Source: Authors.

**Figure 16.** Comparison between waveform obtained for torque from simulation and experimental.



Source: Authors.

## 4. Conclusion

This paper presented a new approach for inductance curve modeling using cubic spline interpolation based on Lagrange polynomials. The proposed model showed excellent estimation precision in both the computer simulations and experimental results. Because it is composed of few coefficients that are processed in the form of polynomials, it was possible to apply the estimator in a low-cost real-time processing system with a DSP as its core. The results demonstrated that the estimator is accurate, robust, and provides a satisfactory solution for the SRM operating as an engine and as a generator. The precision obtained for the inductance derivative also indicates that the proposed estimator is suitable for operations that require the estimation of torque, flux, or other related quantities.

The use of the methodology proposed in this article makes it possible to implement controls for SRM without the need for additional sensors or sophisticated equipment. From the results obtained, it will be possible to apply torque control techniques in electric traction application, direct machine power control in application as a generator, application of control techniques to optimize performance and reduce the oscillating torque.

## Acknowledgments

The authors would like to thank CAPES, CNPq, FAPEMIG, LACE, Federal University of Uberlândia (UFU), Federal Institute of Education, Science and Technology Goiás (IFG), and the National Service for Industrial Learning (SENAI) for their contributions.

## References

- Andrade, D. A. & Krishnan, R. (2001). Characterization of switched reluctance machines using Fourier series approach, Conference Record - IAS Annual Meeting (IEEE Industry Applications Society) 1.
- Banerjee, R. & Sensarma, P. (2018). Non-linear Magnetic Characteristics Modeling for Switched Reluctance Machines, Proceedings of 2018 IEEE International Conference on Power Electronics, Drives and Energy Systems, PEDES 2018, 2018.
- Bilgin B., & Emadi A., & Krishnamurthy M. (2013), Comprehensive evaluation of the dynamic performance of a 6/10 SRM for traction application in PHEVs, IEEE Transactions on Industrial Electronics 60 (2013), 7.
- Bilgin, B. & Jiang, J. (2019). Switched Reluctance Motor Drives - Fundamentals to Applications, CRC Press.
- Bilgin, B., & Jiang, J., & Emadi, A. (2019). Switched Reluctance Motor Drives Fundamentals to Applications, 369.
- Cai, J. & Liu, Z. (2020). An Unsaturated Inductance Reconstruction Based Universal Sensorless Starting Control Scheme for SRM Drives, IEEE Transactions on Industrial Electronics 67(11).

- Cai, Y., et al. (2010). Nonlinear modeling for switched reluctance motor by measuring flux linkage curves, ICCET 2010 - 2010 International Conference on Computer Engineering and Technology, Proceedings, vol. 6.
- Corda J. & Stephenson J. M. (1980). Analytical estimation of the minimum and maximum inductances of a double-salient motor., AIAA Paper.
- Du, J., & Liang, D., & Xu, L. & Li, Q. (2010). Modeling of a linear switched reluctance machine and drive for wave energy conversion using matrix and tensor approach, IEEE Transactions on Magnetics, vol. 46, 2010.
- Duy Minh Nguyen, & D. M., Bahri, I., et al. (2019). Vibration study of the intermittent control for a switched reluctance machine, Mathematics and Computers in Simulation 158.
- Emadi, A., & Joo Lee, Y., & Rajashekara, K. (2008). Power electronics and motor drives in electric, hybrid electric, and plug-in hybrid electric vehicles.
- Fang, G. & Bauman J. (2020). Optimized Switching Angle-Based Torque Control of Switched Reluctance Machines for Electric Vehicles. IEEE, 978-1-7281-4629-4/20.
- Kalaivani, L., & Subburaj, P., & Willjuice I., M. (2013). Speed control of switched reluctance motor with torque ripple reduction using non-dominated sorting genetic algorithm (NSGA-II), International Journal of Electrical Power and Energy Systems 53, no. 1.
- Kushwaha, A. & Kanagaraj, R. (2020) Peak-current estimation using simplified current-rise model of switched reluctance generator operating in single-pulse mode, International Journal of Electrical Power and Energy Systems 120.
- Lin, J., & Cheng K., et al, (2014). Estimation of inductance derivative for force control of linear switched reluctance actuator, IEEE Transactions on Magnetics 50 (2014), no. 11.
- Mikail R., & Husain I., & Islam M. (2013). Finite element based analytical model for controller development of switched reluctance machines, 2013 IEEE Energy Conversion Congress and Exposition, ECCE 2013, 2013.
- Moraes Filho, M. J. d. (2017). Desenvolvimento de plataforma de acionamento digital para motor a relutância variável 8/6. 2017. 98 f. Dissertação (Mestrado em Engenharia Elétrica) - Universidade Federal de Uberlândia.
- Poming, Z. (2020). Magnetic Field Calculation of Switched Reluctance Machines using an improved conformal mapping method. IEEE 19<sup>th</sup> Biennial Conference on Electromagnetic Field Computation, DOI:10.1109/CEFC46938.2020.9451364.
- Rajib. M. & Husain, I. (2013). Finite element based analytical model for controller development of switched reluctance machines, 2013 IEEE Energy Conversion Congress and Exposition, ECCE 2013, 2013.
- Sahoo, S. K., & Panda, S. K. & Xu, J. X. (2008). Piece-wise polynomial based model for switched reluctance motor, IEEE Power and Energy Society 2008 General Meeting: Conversion and Delivery of Electrical Energy in the 21st Century, PES, 2008.
- Song, S. et al (2019). Direct Instantaneous Torque Control of Switched Reluctance Machine Based on Modular Multi-Level power Converter. 22<sup>nd</sup> international conference on electrical machines and systems (ICEMS).
- Takayoshi M., & Jian L., & Eugene P. H., & Thomas A. L. (1997). Self Excited Variable Reluctance Generator. 1997. 5-9, Louisiana : IEE Industry Application Society, 1997, Vol. October.
- Velmurugan, G., & Shen Yeoh, S., & Yang, T., & Bozhko, S. (2019). Piecewise Modelling Approach for Specific Switched Reluctance Machines, Proceedings - ICOECS 2019: 2019 International Conference on Electrotechnical Complexes and Systems.
- Viajante G. P., & Andrade D. A., et al. (2016). A grid connection scheme of a switched reluctance generator for active power injection using P-resonant (P-RES) controller, Electric Power Systems Research; 141:572–9.
- Viajante, G. P. et al. (2018). "Study and Dynamic Performance Analysis of a Switched Reluctance Generator 8/6 for Wind Energy Application," 2018 IEEE International Conference on Environment and Electrical Engineering and 2018 IEEE Industrial and Commercial Power Systems Europe (EEEIC / I&CPS Europe), Palermo, 1-6, 10.1109/EEEIC.2018.8493726.
- Wang, Q., & Chen H, et al., (2016). Inductance estimation method for linear switched reluctance machines considering iron losses, IET Electric Power Applications 10(3).
- Yasa, Y., & Sozer, Y., & Garip, M. (2018). High-speed switched reluctance machine: Natural frequency calculation and acoustic noise prediction, Turkish Journal of Electrical Engineering and Computer Sciences 26, no. 2.